2 Dimensional Electrophoresis Gel Registration Using Point Matching and Local Image-Based Refinement

Mike Rogers[a], Jim Graham[a] and Robert P. Tonge[b]
[a]Imaging Science and Biomedical Engineering,
University of Manchester, Manchester, UK.
[b]Protein Science, Enabling Science and Technology (Biology),
AstraZeneca, Alderley Park, Macclesfield, Cheshire, UK.
mike.rogers@man.ac.uk
http://www.isbe.man.ac.uk/∼mdr/personal.html

Abstract

Recently, proteomics research has become a large growth area in the bio-sciences. Studies involve differential analysis of large sets of 2-D Electrophoresis (2-DE) gels. We present a robust and accurate 2-DE gel alignment algorithm which combines point matching and local image-based refinement. The algorithm uses a novel combination of Euclidian, shape context, image and feature based attributes to produce a point distance measure. Correspondence is determined using this measure and is further improved using an iterative M-estimation approach, and shown to be robust in the presence of large image distortions. Local image-based refinement is shown to improve significantly alignment accuracy. The high accuracy and robustness of the resulting system indicates that it is a promising method for use in practical gel alignment situations.

1 Introduction

Recently, proteomics research has become a large growth area in the bio-sciences. Often, studies involve differential analysis of large sets of 2-D Electrophoresis (2-DE) gels. 2-DE is a method of protein separation that results in a matrix of diffuse spots which can be visualised by pre or post staining. Each of these spots is a separated protein strain. The volume of each spot is proportional to the amount of each protein in the original sample. Figure 1 shows an example of a section from such a gel. In practice, 3,000-4,000 spots can be visualised on a single gel image. The analysis of these complex gel images is a significant bottleneck in the proteomics research workflow [18]. To carry out a differential investigation, it is necessary to determine correspondence between spots on sets of gel images. This implies that a transformation relating one gel image to another is required. The production of 2-DE gels is inherently variable. As a result complex non-linear deformations are often required to align comparable gels. These deformations are often difficult to identify manually and time-consuming to correct. The goal of this work is to develop an image registration scheme that can be used to bring pairs of gels into alignment. However in implementing such a scheme, it is important to retain genuine sample differences between the gel pair.

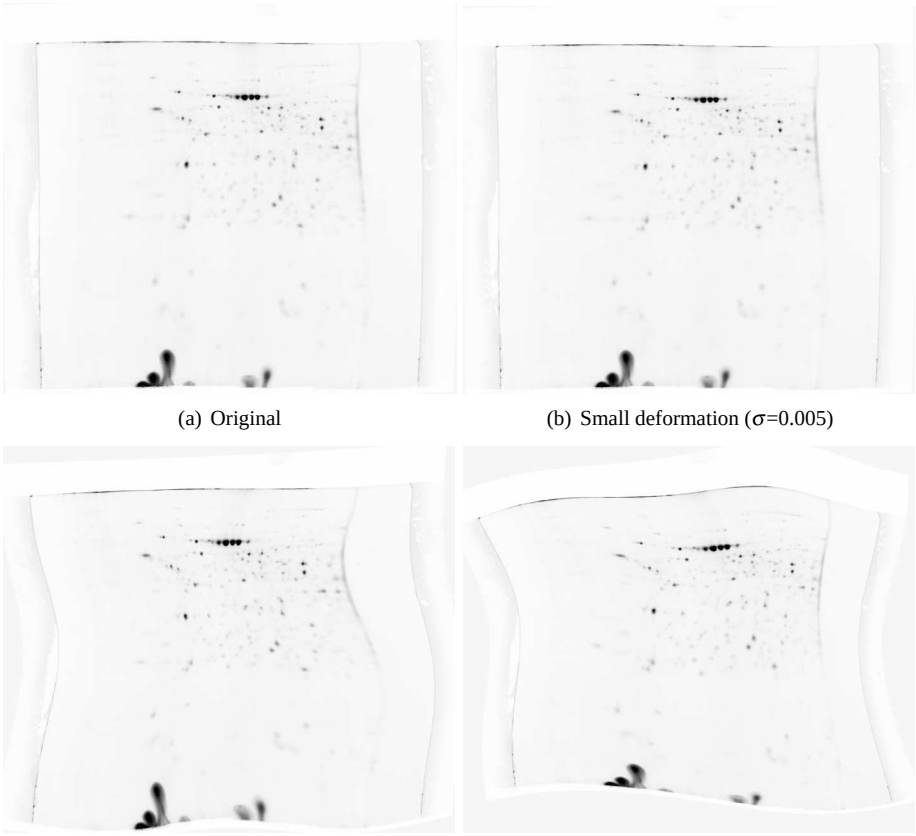

(a) Original (b) Small deformation (σ=0.005)

(c) Medium deformation (σ=0.025) (d) Large deformation (σ=0.05)

Figure 1: Examples of 2-DE gel image. (b)-(d) have been synthetically deformed.

1.1 Background

Many gel matching algorithms algorithms first extract point features from the images, most commonly spot centres, and attempt to match these points. Due to the complexity of gel images, the automatic extraction of point features often introduces additional spurious points whilst missing or, more commonly, merging overlapping spots. As well as these differences, the genuine differences in the patterns of spots in gels can generate non-matching points. These factors create *outlier* points associated with each gel of a comparable pair that have no counterpart in the other. These outliers typically lie within the range of the true spot pattern. Matching algorithms based on point landmarks must be robust to these outliers.

Most commercial systems addressing 2-DE gel matching have used local graph matching algorithms (e.g.[6]). These are generally not robust to outliers and usually require user interaction either to seed the matching process or to verify the final matches. In the computer vision literature, a commonly used point matching scheme is the Iterative Closest Point (ICP) algorithm [2]. ICP iterates between estimating correspondences and then

determining transformation parameters given this correspondence. Standard ICP uses a Euclidian distance metric. Belongie *et al* [1] have proposed a distance metric based on *shape context* (SC), and used it in connection with an optimal Bi-partite Graph Matching (BGM) algorithm to determine correspondence. We have previously shown that BGM is not an appropriate matching algorithm when both sets of points contain outliers [12]. However, it is possible to use SC within the ICP algorithmic framework. In section 2.2 we show how to combine both SC and Euclidian metrics for robust matching. We evaluate this in section 3 together with the *softassign* algorithm of Ranjaragan *et al* [10][11], which has previously been used in building anatomical altases [5]. The use of purely image-based registration (e.g. [14][17]) has not been proved sufficiently robust for gel matching [13]. We have shown [12] that point-matching is more robust for 2-DE gel matching, even in the absence of image information. However, we believe that the use of image-based features can improve the local registration of purely point-based matching.

2 Method

Our gel registration algorithm seeks to combine the global correspondence properties of point matching schemes, with the good local refinement properties of image based registration. First protein spot centre point features are extracted from a pair of images. These points are corresponded using a distance metric combining Euclidean distance, the context of neighbouring spot positions and the context of the distribution of spot intensity and size. The transformation parameters arising from this match are calculated and refined using local image correlation. The resulting transformation is used to initialise and constrain the next point matching step. The process is iterated until a convergence criterion is met. The stages of our algorithm are described in more detail in sections 2.1-2.4.

Throughout the process we have used Clamped-Plate Splines (CPSs) [16] to parameterise non-rigid transformations, after extracting any affine component. CPSs are interpolating spines, similar to Thin-Plate Splines [3], but they use an alternative Green's function that yields improved boundary conditions on the unit circle. With n control points $\{(x_i,y_i)\}_{i=1}^{n}$, CPS $\vec{a}$ and affine parameters $\vec{b}$ can be calculated by solving the linear system:

$$\vec{z} = A\vec{a} + B\vec{b} \tag{1}$$

where $\vec{z}$ are spline target points, A is an $n \times n$ matrix of Green's function values ($A_{ij} = G(\|x_i - x_j, y_i - y_j\|)$) and B is an $n \times 3$ matrix whose rows are $[1 x_i y_i]$. They can be converted into weighted smoothing splines by modifying the above formula:

$$\vec{w}\vec{z} = (A' + \lambda I)\vec{a} + B'\vec{b} \tag{2}$$

where $\vec{w}$ is an n element vector of control point weights, A' is an $n \times n$ matrix of weighted Green's function values ($A'_{ij} = G(\|w_i x_i - w_j x_j, w_i y_i - w_j y_j\|)$) and B' is an $n \times 3$ matrix whose rows are $[1 (w_i x_i) (w_i y_i)]$. In 2, $\lambda > 0$ is a smoothing parameter and I is the $n \times n$ identity matrix. We chose to manipulate λ as a function of p: $\lambda = p/(1-p)$, in which case $0 \leq p < 1$, with $p = 0$ representing an interpolating spline (no smoothing) and $p \to 1$ increases smoothing until only affine parameters are obtained. All transformations have been calculated in the range $-0.5 \to 0.5$, scaling and centring image coordinates to this region.

The whole algorithm has been implemented in a multi-resolution framework, with the final transform from the current resolution being used to initialise the next highest. To

help avoid local minima we have varied the amount of regularisation applied during spline calculation at each resolution. Starting with a strongly constrained smooth transform at coarse resolutions, the value of p is decreased at each resolution level, ending with a less constrained transform. In this work we vary p linearly between 0.25 and 0.01. This approach, controlling regularisation as the refinement progresses is similar in effect to the linkage between regularisation and temperature schedule in the work of Chui *et al* [5].

We now describe each stage of our algorithm in more detail.

2.1 Feature Extraction

We have used an extremely simple point feature extraction process to detect spot centres at each resolution. We are able to do this as the rest of the algorithm has been designed to be robust to large numbers of outliers and noise in the original point sets. To calculate a binary image feature image, we use a threshold on the Laplacian of each image as follows:

$$f = (\partial_x^2 > t) \wedge (\partial_y^2 > t) \tag{3}$$

where ∂_x^2 and ∂_y^2 are the 2nd derivative of the Gaussian smoothed gel image in the x and y directions respectively and t is a threshold. We have chosen to smooth with Gaussian $\sigma = 2$ pixels and threshold at $t = 0$. The centre of gravity of each connected region in the image meeting this criterion is taken as a point location. We have limited the number of points to a maximum by discarding all but the 400 most intense spots, measured using image intensity information. The number of features to retain was chosen manually. Our spline transformation model therefore has a maximum of 400 control points.

2.2 Point Matching

In previous work, we have developed a point matching strategy suitable for use when aligning gel images [12]. In this work, we have extended the basic scheme in several ways, and we will now briefly describe the algorithm together with our extensions.

Our point matching scheme is based on the commonly used ICP algorithm [2]. In [12] we used the SC [1] measure as an alternative distance metric to Euclidian distance. SC provides a semi-global description of the spatial distribution of neighbouring points by counting the number of points in radial regions, yielding histograms that can be made invariant to affine deformations (see figure 2(a)). The method also includes an explicit treatment of outliers. The χ^2 statistic between histograms is used as a distance between features. Careful evaluation in the presence of outlier features has shown that when deformation is expected to be large the most appropriate distance measure is SC, and when deformation is small Euclidian (Euc) distance yields the highest accuracy and robustness [12]. For this reason, we have chosen to use a weighted sum of the two distance measures:

$$d = \alpha d_{Euc} + (1 - \alpha) d_{SC} \tag{4}$$

where α is a weighting factor between the two measures. Both are normalised over the set of all distances to have mean 0 and standard deviation 1, which ensures equal influence for each measure when $\alpha = 0.5$.

In addition to the distance measure presented in [12], we have added two more attributes. Following the SC histogram binning method, we have developed semi-global image intensity and feature information descriptors. As illustrated in figures 2(b) and 2(c), rather than counting the number of feature points in a specific bin, we have used

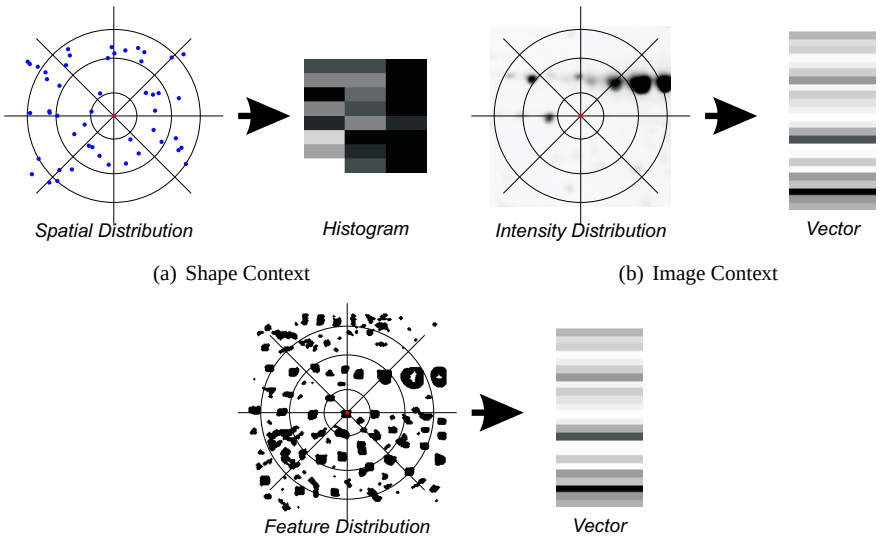

(a) Shape Context (b) Image Context

(c) Feature Context

Figure 2: Attributes for feature distance calculation.

the average image intensity within the region as an element of an attribute vector. The Euclidian distance between these vectors can be calculated as a feature distance measure. However, we know there will be important genuine differences between the intensities and patterns of spots in two gels. This makes Euclidian intensity distance an inappropriate measure. Instead, we have the robust Least Median of Squares (LMedS) measure to calculate the distance between vectors. Using this scheme, we produce two additional distance measures, one associated with the original image intensities (figure 2(b)) and another associated with the binary feature image (figure 2(c)) calculated during feature extraction. The former we term Image Context (IC) and contains information about the intensities of features surrounding each point, the later termed Feature Context (FC) encapsulates information about the extent of the features. These measures are combined into a single distance between features using the following formula (neglecting normalisation):

$$d' = \alpha d_{Euc} + (1-\alpha)(d_{SC} + d_{IC} + d_{FC})/3 \quad (5)$$

where d_{IC} and d_{FC} are distances calculated using LMedS.

Using a closest point method with this distance measure, correspondence can be determined between feature points. Corresponding points are used as control points to estimate CPS parameters. Due to genuine differences in spot pattern and our basic automatic feature extraction scheme we know that correspondences will contain errors. We have used the iterative M-estimation paradigm to down-weight correspondences that are inconsistent with their neighbours. M-estimation calculates weights for each data point based on their residual distance against a model. In our case, residuals are calculated as the Euclidian distance between the predicted position of the feature given by the regularised CPS transform and the associated corresponding point position. We have used the Huber kernel [7] to weight the correspondences. CPS parameters are re-calculated from weighted

correspondences using equation 2. The process is iterated until convergence.

2.3 Local Image-Based Refinement

A further refinement to [12] addresses the inaccuracy of feature localisation using the centre of gravity of regions within the binary feature image. The centre of gravity of corresponding feature areas in two different gels may not be in the same position on the gels. For this reason, we optimise the position of each point in one image w.r.t. the location of corresponding point in the other. A simple gradient descent process minimises the cross-correlation between local image patches centred at the location of each corresponding pair of points, by adjusting the location of a point in one of the images. This process is applied following the determination of correspondence and transformation parameters, on corresponding feature pairs with high weight at each resolution level. The new feature locations are used in subsequent feature matching iterations. For this work, we have used an image region of 15×15 pixels, corresponding to an image region slightly larger than the largest expected protein spot.

2.4 Convergence Criterion

The criterion chosen to determine algorithm convergence is difficult to define. At present we simply use the mean weighted Euclidian distance between corresponding features (determined in 2.2). If the difference between this value at successive iterations is less than 10^{-6} then the algorithm is said to have converged. Further work is required to determine if this an appropriate criterion.

We have also observed that after approximately three passes through point matching and local refinement at any resolution level little improvement in registration quality is achieved. For this reason, we apply a maximum of three algorithm iterations at each resolution.

3 Evaluation

We have evaluated our point matching algorithm, both with and without local image refinement, in comparison with the softassign approach described in [5].

As subsequent analysis of 2-DE gels requires the comparison of corresponding protein spots, the effectiveness of gel matching algorithms should be measured in terms of the accuracy of alignment of protein spots. To perform this evaluation we require a large set of gel image pairs with annotated spot positions and known correspondence. Ideally, matching difficulty for each pair should be known and should represent the true range found in real data. Data meeting these requirements is not available and, due to the complexity of the images, would be extremely time consuming to produce. Instead, we have used DIGE gel pairs with known spot locations and introduced varying amounts of synthetic deformation to form our test data set. DIGE gels [15] are produced using protein mixtures that are pre-stained with different fluorescent dyes. The dyes are chosen to fluoresce under different frequencies of UV light. After staining, up to three samples can be mixed together and run on a single gel. Corresponding proteins from different samples will migrate to exactly the same place on the gel and be coincident in gel images. To retrieve images from the separate samples, the gel is illuminated with the excitation frequency for each of the dyes, allowing pairs of images to be produced with perfect correspondence but showing genuine sample differences[1].

[1] Gel matching is still required to compare between different DIGE gel pairs!

In this evaluation, we have used 5 pairs of DIGE gel images, each with $\sim$650 annotated spot positions. Using these images, we created a large evaluation data set by introducing varying amounts of synthetic deformation to one of the images of each pair. The amount of deformation has been controlled as follows: 10 control points are sampled from a uniform random distribution. 10 random offsets are sampled from a Gaussian with known σ. A smooth Gaussian RBF transformation ($p = 0.05$) is calculated using the control points and offsets and used to transform a gel image and its spot positions. Increasing the value of σ increases the amount of deformation. An estimate of the deformation energy E can be calculated from the parameters of the RBF ($E = \sum \mathtt{diag}(\vec{a}' A \vec{a})$). Figure 1 shows examples of images deformed using different values of σ. In our evaluation, σ has been varied linearly in 10 steps between $0.005 \rightarrow 0.05$ ($E : 0.0061 \rightarrow 1.2$). By observation, the top end of this range greatly exceeds the maximum amount of deformation required to align corresponding gels in practice. At each value of σ, we have created 5 randomly deformed images from each DIGE pair. This gives a total of $5 \times 5 \times 10 = 250$ gel alignments, each with $\sim$650 spots.

After gel alignment, the recovered transformation[2] is used to transform the spot locations to their estimated position in the un-deformed gel. We have measured the residual Euclidian distance between the transformed spots and their ground-truth position (r). Residual r is reported as a proportion of the maximum dimension of the associated gel image. In this way, $r = 0.01$ represents an error of 1% of image size.

4 Results and Discussion

Figure 3(a) shows mean and standard deviation of r after alignment for each algorithm: Point Matching with Refinement (PMR), Point Matching (PM) and SoftAssign (SA)[3]. The results are plotted against mean deformation energy (E) over replicates at each value of σ. A residual value of $r = 0$ indicates a perfect recovery of the alignment of a protein spot. Results for the set of 5 images have been combined and as such each data point represents $\sim$16250 point residuals. Also shown in figure 3(a) are values for un-aligned point residuals (Orig) showing the amount of deformation in the original data in terms of point residual. The data for PM and PMR are almost coincident on the scale of figure 3(a). Figure 3(b) shows the same data, this time including only the first 7 groups for PM and PMR. Large error bars on groups $8 \rightarrow 10$ prevent easy visual comparison of group means, and so have not been displayed on this figure.

Each algorithm produces reduced residuals compared to the original deformations. However, the performance of SA is far worse than either PM or PMR. Throughout the SA algorithm uncertainty over correspondence is gradually reduced using a deterministic annealing schedule. One-to-one correspondence can be forced by reducing the annealing temperature to zero. However, in the implementation of SA we have used, temperature is coupled to spline regularisation, and allowing temperature to reach 0 produces unstable results. This problem could be resolved using a fully diffeomorphic transformation parametrisation such as that proposed in [9]. In this evaluation, we have used the annealing parameters provided with the implementation that were used to produce results reported in [5]. These parameters retain a certain level of correspondence uncertainty in the estimation of the final transform. This uncertainty reduces the accuracy of the algorithm. In contrast, both PM and PMR algorithms use one-to-one correspondence, it-

[2] A thin-plate spline is used to parameterise transformations in [5]

[3] Using code available at: http://noodle.med.yale.edu/$\sim$chui/tps-rpm.html

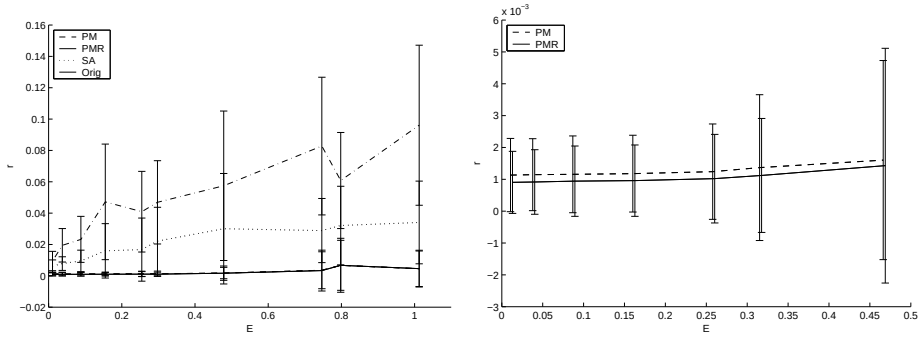

(a) (b)

Figure 3: (a) Mean residual r for each algorithm (PM,PMR,AS) and original deformation (Orig) with ± 1 std.dev. error bars. r plotted as a proportion of image size. x-axis shows mean deformation energy $\bar{E}$ for the original deformation of each group. (b) Same data, showing only first 7 measurements for PM and PMR (error bars slightly offset for display).

eratively down-weighting inconsistent correspondences. This allows greater accuracy to be achieved when a large enough proportion of correct correspondences are represented in the original set. Our careful choice of distance measure ensures that this proportion is large. Also, SA may only be well suited to highly structured data (such as that presented in [5]). SA has been observed to first align along the *principal modes* of point patterns, which may be of limited utility in this case.

Both PM and PMR are significantly more accurate than SA. Figure 3(b) shows that PMR, which uses local image refinement, produces consistently lower residuals than PM. The reduction in residual mean is significant at the 0.01 level for all groups, except when $\sigma = 0.045 (\bar{E} \approx 0.75)$. The mean residual achieved by both methods is almost constant up to a bending energy of $\bar{E} \approx 0.25$, showing robustness to deformations up to this magnitude. We have observed that this is a realistic upper level for the amount of deformation required to align most 2-DE gel pairs, however further work is required to validate this. PM and PMR give a residual value of $r \approx 10^{-3}$ for the $\bar{E} \approx 0.25$ group, which corresponds to a mean protein spot location residual of 1 pixel in a 1000×1000 pixel image.

For a gel registration system to be of use in practice, alignment must be accurate across the entire gel. If groups of misaligned spots are present manual validation and correction of results would be required. This is a time-consuming and subjective process which should be avoided. We have evaluated the numbers of large point residuals by counting the number of residuals greater than a threshold. Tables 1(a) and (b) show the percentage of residuals larger than 1% and 2% of image size for a selection of values of $\bar{E}$. For users to have high confidence in a gel alignment system, very few large residuals must be produced. Using 1% of image size (10 pixels in a 1000×1000 pixel image) as a threshold, both PM and PMR produce fewer than 45 large residuals out of ~ 16500 measurements. Using the 2% threshold both produce less than 10 large residuals. In contrast, SA results in ~ 780 and ~ 1400 respectively. The small numbers of large residuals produced demonstrates that either PM or PMR may be suitable for use for automatic gel

$\bar{E} \approx$	0.01	0.08	0.25	1.02
PM	0.15	0.015	0.26	11.29
PMR	0.02	0.013	0.21	10.28
SA	64.93	71.33	84.1	93.77

(a) $r > 1\%$ image size

$\bar{E} \approx$	0.01	0.08	0.25	1.02
PM	0	0.01	0.04	8.19
PMR	0	0.01	0.07	7.72
SA	15.62	30.94	48.54	79.35

(b) $r > 2\%$ image size

Table 1: Percentage of residuals greater than 1% and 2% of image size.

alignment.

5 Conclusion and Future Directions

We have presented a robust and accurate point matching based 2-DE gel alignment algorithm. The algorithm uses a novel combination of Euclidian, shape context, image and feature based attributes to produce a point distance measure capable of determining good correspondence between protein spot point sets. This correspondence is further improved using an iterative M-estimation approach. Adding a local refinement step based on image intensities has been shown to improve significantly alignment accuracy. Our algorithms have been shown to out-perform the softassign approach described in [5]. The high accuracy of the system together with the small number of large spot alignment errors indicates that this system shows promise for use in practical gel alignment situations.

The algorithm described in this paper may be improved in several ways. The effect of the choice of the number of spline control points has not been investigated. The issue of group-wise gel alignment has not been addressed in this work. In particular, the alignment method presented is not inverse consistent. The work of Christensen [4] could be used to enforce this constraint. Also it would be possible to ensure diffeomorphic transformations are produced using [9].

Recently, interest has grown in combining point based and image based alignment techniques. The point matching scheme presented here could be used to avoid the manual landmark placement and correspondence requirements of [8][13].

References

[1] S Belongie, J Malik, and J Puzicha. Shape matching and object recognition using shape context. *IEEE Transactions on Pattern Analysis and Machine Intelligence*, 24(4):509–522, April 2002.

[2] P J Besl and H D McKay. A method for registration of 3-d shapes. *IEEE Transactions on Pattern Analysis and Machine Vision*, 14(2):239–256, 1992.

[3] F L Bookstein. Principal warps: Thin-plate splines and the decomposition of deformations. *IEEE Transactions on Pattern Analysis and Machine Intelligence*, 11(6):567–585, 1989.

[4] G E Christensen. Inverse consistent registration with object boundary constraints. In *Proceedings of the International Symposium on Biomedical Imaging*, pages 591–594, Arlington, VA, USA, 2004.

[5] H Chui, A Rangarajan, J Zhang, and C M Leonard. Unsupervised learning of an atlas from unlabeled point-sets. *IEEE Transactions on Pattern Analysis and Machine Intelligence*, 26(2):160–173, February 2004.

[6] F Hoffman, K Kriegal, and C Wenk. An applied point pattern matching problem: Comparing 2d patterns of protein spots. *Discrete Applied Mathematics*, 93:75–88, 1999.

[7] P J Huber. *Robust Statistics*. Wiley, New York, 1981.

[8] H J Johnson and G E Christensen. Consistent landmark and intensity-based image registration. *IEEE Transactions on Medical Imaging*, 21(5):450–461, 2002.

[9] S C Joshi and M I Miller. Landmark matching via large deformation diffeomorphisms. *IEEE Transactions on Image Processing*, 9(8):1357–1370, August 2000.

[10] A Ranagarajan, H Chui, E Mjolsness, S Pappu, L Davachi, P Goldman-Rakic, and J Duncan. A robust pattern matching algorithm for autoradiograph alignment. *Medical Image Analysis*, 1(4):379–398, 1997.

[11] A Rangarajan, H Chui, and J S Duncan. Rigid point feature registration using mutual information. *Medical Image Analysis*, 4:1–17, 1999.

[12] M Rogers, J Graham, and R P Tonge. 2-d electrophoresis gel registration using feature matching. In *Proceedings of the IEEE International Symposium on Biomedical Imaging*, pages 1436–1439, Arlington, USA, April 2004.

[13] K Rohr, P Cathier, and S Wörz. Elastic registration of electrophoresis images using intensity information and point landmarks. *Pattern Recognition*, 37:1035–1048, 2004.

[14] Z Smilansky. Automatic registration for images of two-dimensional protein gels. *Electrophoresis*, 22:1616–1626, 2001.

[15] R Tonge, J Shaw, B Middleton, R Rowlinson, S Rayner, J Young, F Pognan, E Hawkins, I Currie, and M Davison. Validation and development of flourescence two-dimensional differential gel electrophoresis proteomics technology. *Proteomics*, 1:377–396, 2001.

[16] C Twining, S Marsland, and C J Taylor. Measuring geodesic distances on the space of bounded diffeomorphisms. In *BMVC*, volume 2, pages 847–856, 2002.

[17] S Veeser, M J Dunn, and G-Z Yang. Multiresolution image registration for two-dimensional gel electrophoresis. *Proteomics*, 1:856–870, 2001.

[18] T Voss and P Haberl. Observations on the reproducability and matching efficiency of two-dimensional electrophoresis gels: Consequences for comprehensive data analysis. *Electrophoresis*, 21:3345–3350, 2000.